ACS APPLIED MATERIALS & INTERFACES

RESEARCH ARTICLE

www.acsami.org

Sodium Fluoride-Assisted Modulation of Anodized TiO_2 Nanotube for Dye-Sensitized Solar Cells Application

Jung-Ho Yun,[†] Yun Hau Ng,[†] Changhui Ye,[‡] Attila J. Mozer,[*,§] Gordon G. Wallace,[§] and Rose Amal[*,†]

[†]ARC Centre of Excellence for Functional Nanomaterials School of Chemical Engineering, The University of New South Wales, Sydney NSW 2052, Australia

[‡]Key Laboratory of Materials Physics, Institute of Solid State Physics, Chinese Academyof Sciences, Hefei, China

[§]Intelligent Polymer Research Institute, ARC Centre of Excellence for Electromaterials Science, University of Wollongong, Wollongong NSW 2522, Australia

Supporting Information

ABSTRACT: This work reports the use of sodium fluoride (in ethylene glycol electrolyte) as the replacement of hydrofluoric acid and ammonium fluoride to fabricate long and perpendicularly well-aligned TiO_2 nanotube (TNT) (up to 21 μm) using anodization. Anodizing duration, applied voltage and electrolyte composition influenced the geometry and surface morphologies of TNT. The growth mechanism of TNT is interpreted by analyzing the current transient profile and the total charge density generated during anodization. The system with low water content (2 wt %) yielded a membrane-like mesoporous TiO_2 film, whereas high anodizing voltage (70 V) resulted in the unstable film of TNT arrays. An optimized condition using 5 wt % water content and 60 V of anodizing voltage gave a stable array of nanotube with controllable length and pore diameter. Upon photoexcitation, TNTs synthesized under this condition exhibited a slower charge recombination rate as nanotube length increased. When made into *cis*-diisothiocyanato-bis(2,2-bipyridyl-4,4-dicarboxylato) ruthenium(II) bis (tetrabutyl-ammonium)(N719) dye-sensitized solar cells, good device efficiency at 3.33 % based on the optimized TNT arrays was achieved with longer electron time compared with most mesoporous TiO_2 films.

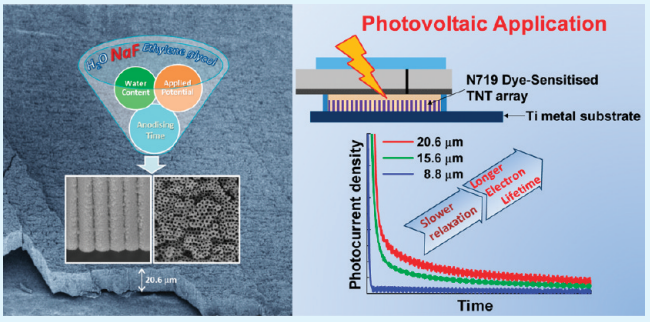

KEYWORDS: sodium fluoride, anodization, well-aligned TiO_2 nanotube, photoelectrochemistry, dye-sensitized solar cell

INTRODUCTION

Because of the suitable band-gap energy, good chemical and thermal stability, ease of morphological and structural control, and its abundance, titanium dioxide (TiO_2) has become one of the most promising semiconducting materials for use in energy related applications. Existing synthetic methods have successfully prepared TiO_2 with various structures such as mesoporous particulates, hollow spheres, nanorods and nanotubes.[1−5] Applications of these TiO_2 structures have been extensively reported, especially in photocatalysis, water photoelectrolysis and solar cell applications.[5−9] In dye-sensitized solar cells (DSSCs), the use of mesoporous nanocrystalline TiO_2 has been found to enhance photocurrent generation because of its higher dye-uptake originating from the high available surface area.[1] However, electron transport in this randomly oriented TiO_2 mesoporous structure is limited by the existence of grain boundaries that act as charge recombination centers. The fabrication of vertically oriented and highly ordered TiO_2 nanotubes (TNT) via electrochemical anodization of titanium (Ti) should alleviate recombination, while sustaining a large surface area for dye-uptake. The latter attribute arizes from the interior and exterior surface of the TNT wall.

Fabrication of TNT arrays using electrochemical anodization has been widely studied.[10−14] In general, a source of fluoride ion (F^-) is required in the electrolyte during anodization in order for the dissolution of the TiO_2 to initiate pore formation. Hydrofluoric acid (HF) and ammonium fluoride (NH_4F) are the most widely employed fluorides due to their ability to provide a high level of dissolution in both aqueous and non-aqueous electrolytes.[10,12] Schmuki and co-workers successfully prepared TNT arrays with controllable geometry using HF-containing aqueous electrolyte; 3.8% of energy conversion efficiency has been achieved on the DSSCs made of these TNT arrays.[15,16] Extremely long TNT with 220 μm in length has also been synthesized in an organic-based NH_4F electrolyte and has found uses in backside illuminated photovoltaic.[17,18] However, the use of HF and NH_4F raises both safety and environmental concerns. The substitution of these harmful fluoride sources with a more environmentally benign NaF is attractive. The increased safety arising from use of NaF is evident by the usage of this material in drinking water fluoridation.[19]

To date, the application of NaF in the fabrication of TNT arrays has only been reported in aqueous electrolyte.[12,20] Under

Received: February 2, 2011
Accepted: April 11, 2011
Published: April 11, 2011

aqueous electrolyte system, however, limited growth of TNT (~3 μm) was observed due to the rapid dissolution of TiO_2 by the H^+ and F^- ions formed in the water. The length of TNT is crucial in DSSCs as it determines the total amount of dye-uptake and in turn the energy conversion efficiency. The challenge to obtain longer TNTs using NaF is in achieving a dynamic equilibrium between TNT growth and dissolution processes that ensure a continuous growth of TNTs. Herein, we describe the formation of a vertically aligned and well-ordered TNT array using electrochemical anodization of Ti foil under a non-aqueous (ethylene glycol) electrolyte containing NaF. Geometry of TNT arrays, including nanotube length, pore diameter and surface roughness, can be conveniently controlled by optimizing the composition of the electrolyte and the anodizing parameters. Its physical, optical, and photoelectrochemical properties are investigated. In addition, the TNT array was fabricated into an N719 ruthenium-based DSSC device. The electron lifetime, diffusion coefficient, and open circuit voltage of the most optimized TNT is carefully evaluated.

EXPERIMENTAL SECTION

Anodization of TNT Array. The TNT array was prepared by anodizing Ti foil (99.7 %, Aldrich) with 20 × 20 × 0.127 mm dimension in ethylene glycol based fluoride electrolyte. The Ti foils were first cleaned with acetone in mild sonication and Milli-Q water followed by vacuum drying before anodization. The electrolytes were prepared by mixing ethylene glycol (> 99 %, Aldrich) and 0.5 wt % of NaF (99 %, Ajax Chemicals) with water varied from 2 to 50 wt %. A two-electrode system was used for anodization, with Ti foil as the anode, and platinum plate and wire as the cathode. An in-house designed sealed anodic cell was used as the reactor. A constant distance was maintained between electrodes, and the area of anode exposed to the electrolyte was controlled. A programmable DC power supply (PST-3201, GW Instek) interfaced with a computer was used to monitor the anodization current density. An applied potential between 20 and 70 V and an anodization time between 1 and 15 h were employed. After anodization, the TNT array samples were rinsed with Milli-Q water in a sonication bath to remove debris of broken tubes, and dried at 110 °C for 1 h, followed by calcination at 450 °C for 3 h with a ramping rate of 5 °C min^{-1} in air. Although calcination at higher temperature (> 580 °C) would enhance the structural stability of the TNT arrays, they transform to rutile phase. Our previous work indicated that anatase is the preferred phase for better charge-transport properties.[21]

Characterizations of TNT Array. The TNT morphologies, including nanotube length, pore diameter, and wall thickness, were determined using a scanning electron microscope (SEM, S900, Hitachi). Crystallinity and phases of TNT were analysed using an X-ray diffractometer (X'pert Pro MRD, Philips). The surface elemental analysis of TNT was performed on an X-ray photoemission spectrometer (XPS, ESCALAB220i-XL, Thermo Scientific) with Al K alpha at 1486.6 eV. The optical band-gap energy of the TNT array was determined through a diffused reflectance UV spectrophotometer (Cary 300, Varian).

A three-electrode photoelectrochemical (PEC) cell consisting of a TNT working electrode, platinum counter electrode and Ag/AgCl reference electrode was used for PEC measurement. The photocurrent density and photocurrent transient responses were measured using a potentiostat (PG STAT-302N, Autolab) with GPES analyzing software. All PEC measurements of TNT were performed using a 300W xenon arc lamp source with 0.1 M of Na_2SO_4 under argon gas purging with stirring.

Fabrication of DSSCs with TNT Array. The TNT arrays (6 × 6 mm) obtained from 15 and 3 h of anodization at 60 V with ethylene glycol containing 0.5 wt % NaF and 5 wt % H_2O were integrated into a DSSC device. Prior to dye adsorption, the TNT array was treated with 0.04 M of $TiCl_4$ at 70 °C for 30 min followed by rinsing with water. $TiCl_4$ treated TNT was calcined at 450 °C for 3 h and reheated at 450 °C for 30 min if not immediately used. The TNT array was soaked in a 0.3 mM N719 (*cis*-diisothiocyanato-bis(2,2-bipyridyl-4,4-dicarboxylato) ruthenium(II) bis (tetrabutyl-ammonium)) dye solution in anhydrous acetonitrile for 18 h. N719 compound was purchased from Sigma-Aldrich. A sandwich-type DSSC was assembled using the dye-sensitized TNT array as a photoanode and platinum-deposited ITO counter electrode separated by a sealant (Surlyn 60 μm thickness, Solaronix). The electrolyte was a mixture of 0.1 M LiI, 0.6 M 1, 2-dimethyl-3-propylimidazolium iodide (DMPII), 0.03 M I_2, and 0.5 M t-butylpyridine (TBP) in acetonitrile. The electrolyte was injected to the cell through a hole drilled through the counter electrode with the aid of a vacuum. The photovoltaic properties were measured under a calibrated AM 1.5 solar simulator at 100 mW cm^{-2} light intensity.

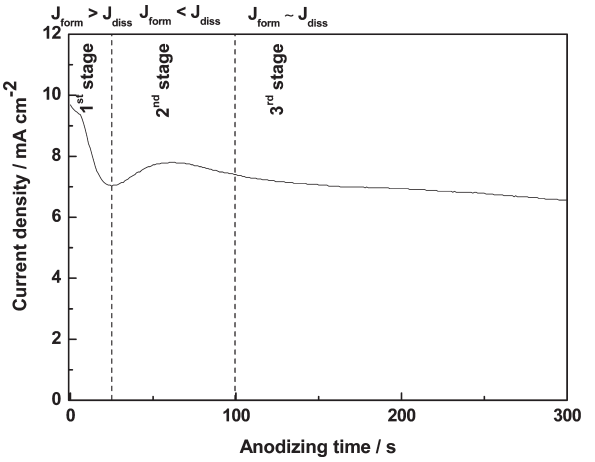

Figure 1. Typical current profile during anodization of Ti foil in ethylene glycol electrolyte containing 0.5 wt % NaF.

RESULTS AND DISCUSSION

Mechanistic Growth of TNT. Figure 1 shows a typical profile of the current transient recorded during the anodization of Ti foil in ethylene glycol containing NaF. For all conditions studied here, anodization of Ti foil to form nanotubes followed three different stages. In the first stage, the current decayed within the first minute of the anodization. This is attributed to oxidation of Ti foil to form a compact layer of TiO_2. As the formation of thin TiO_2 layer covered the area of exposed Ti foil, the further oxidation of Ti slowed down, resulting in the current decay. Subsequently, when chemical dissolution of the TiO_2 passive layer by fluoride started to take place which render more Ti to undergo anodic oxidation, a temporary rebound in current (second stage) is observed. In the third stage, formation and dissolution of TiO_2 occurred concurrently and competitively, which gradually led to steady state current generation. In general, the formation and growth of TNT relies on two main fundamental reactions: sustained oxidation of the Ti metal and pore growth by chemical dissolution of the formed titanium oxide, as expressed by the two equations below.

$$Ti + 2H_2O \rightarrow TiO_2 + 4H^+ + 4e \quad (1)$$

$$TiO_2 + 6F^- + 4H^+ \rightarrow [TiF_6]^{2-} + 2H_2O \quad (2)$$

Therefore, the changes in the current density profile could be used to describe the reaction, which dominates during the

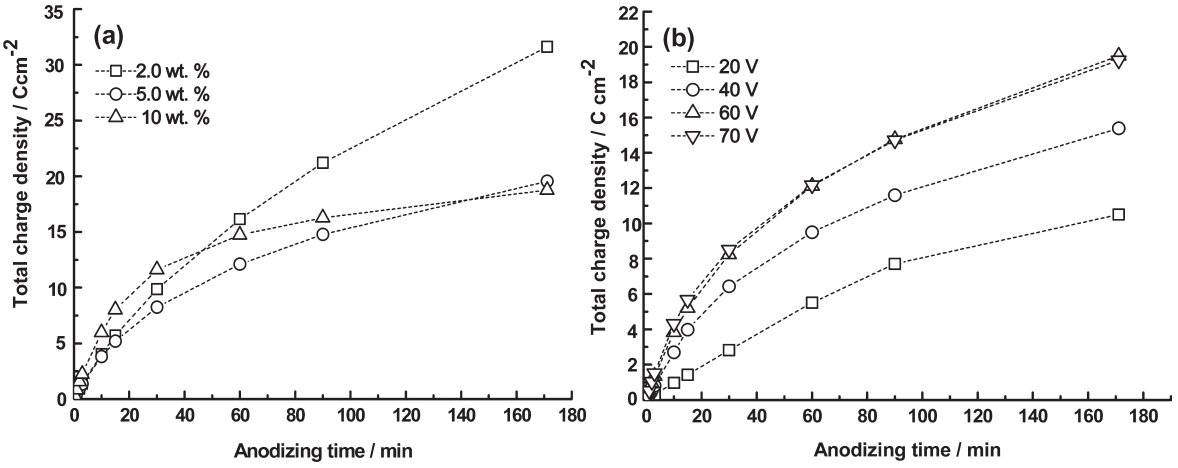

Figure 2. Total charge density for anodized Ti foil during 3 h anodization under (a) different water content with 60 V applied voltage, and (b) different applied voltage condition with 5 wt % water concentration in electrolyte.

anodizing process.[22] Considering the predominant reaction indicated at each stage, the current density observed in the experiment (J) can be defined as the total current generated or influenced by the formation of an anodic layer (J_{form}) and the dissolution of TiO_2 (J_{diss})

$$J = J_{form} + J_{diss} \quad (3)$$

Effect of Water Content and Anodic Potential. Figure 2 shows the total charge density of Ti foil anodized under different experimental conditions, which were calculated by integrating the total area of the current transient profile as shown in Figure 1 using the following equation

$$\text{total charge density}(\text{C cm}^{-2}) = \int_0^t j dt$$

where total charge density is the amount of charge in coulomb, j is the current density in mA cm^{-2}, and t is anodizing time in seconds. Total charge density represents the overall rate of the anodizing process. Figure 2a shows the total charge density of Ti anodized with different water contents in the electrolyte. All samples indicated a rapid initial anodization process followed by a gradual decrease in the reaction rate. Although the system with 10 wt % water anodized faster in the first 20 min, the total charge density generated for the whole anodization duration was small. This is due to the continuous breakdown of the TNT structure during growth as higher water content induces greater dissolution of TiO_2. Although the total charge densities generated by the sample with 5 and 10 wt % water content were comparable, the TNT arrays produced had markedly different lengths: 8.77 μm (5 wt %) and 3.26 μm (10 wt %). Therefore, even with the similar overall anodizing rate as indicated in the total charge density, the growth of the TNT arrays is also subjected to the dominancy of either J_{form} or J_{diss}. In this case, the system with 5 wt % water possesses greater J_{form} than J_{diss} ($J_{form} > J_{diss}$), and vice versa for the system with 10 wt % water. According to the total charge density, the TNT array derived from 2 wt % water has the longest length of TNT, as expected. Figure 2b shows plots of total charge density of TNT arrays obtained under different applied potentials. In general, total charge density is proportional to the applied potential, i.e. higher applied potential induces a faster anodization process. The total charge density (overall rate of anodization) achieved a saturation state at 60 V; a potential higher than that did not further increase the total charge density. Although 70 V did not generate a higher total charge density compared to that of the 60 V, the length of nanotube obtained at 70 V (10.60 μm) was longer than that obtained at 60 V (8.77 μm). Again, this indicates the difference in ratio of J_{form} and J_{diss} induced by the different applied voltage, where J_{form} is promoted by a higher potential.

Table 1. Geometry of TNT Anodized at Various Water Content and Applied Potentials in Ethylene Glycol Containing 0.5 wt % NaF

water concentration (wt %)	applied potential (3 h) (V)	length of TNT layer (μm)	pore diameter (nm)	wall thickness (nm)
2.0	60	9.1	65.1	21.3
5.0	60	8.8	74.5	32.7
10.0	60	3.3	89.9	35.8
50.0	60	N.T.[a]	N.T.[a]	N.T.[a]
5.0	20	0.9	N.O.[b]	N.O.[b]
5.0	40	4.1	55.0	30.5
5.0	60	8.8	74.5	32.7
5.0	70	10.6	80.4	32.7

[a] No tubes. [b] Not observed.

Table 1 summarizes the geometry properties of TNT arrays prepared under various experimental conditions. Nanotube length is inversely proportional to water content in the electrolyte as the presence of water promotes a higher degree of TiO_2 chemical dissolution, resulting in a broken/shorter nanotube. When water concentration was very high (50 wt %), TiO_2 particles were formed instead of a TNT array (please see Figure S1 in the Supporting Information). In addition, nanotube length, pore diameter, and thickness of the nanotube wall were found to increase with the applied potential.

Figure 3 presents a top view and cross-sectional SEM images of the TNT arrays prepared with different water concentrations at 60 V. When the water content was low (2 wt %), well-defined nanotubes were not developed, i.e., the spaces between the individual tube were not formed. Instead, it reveals the

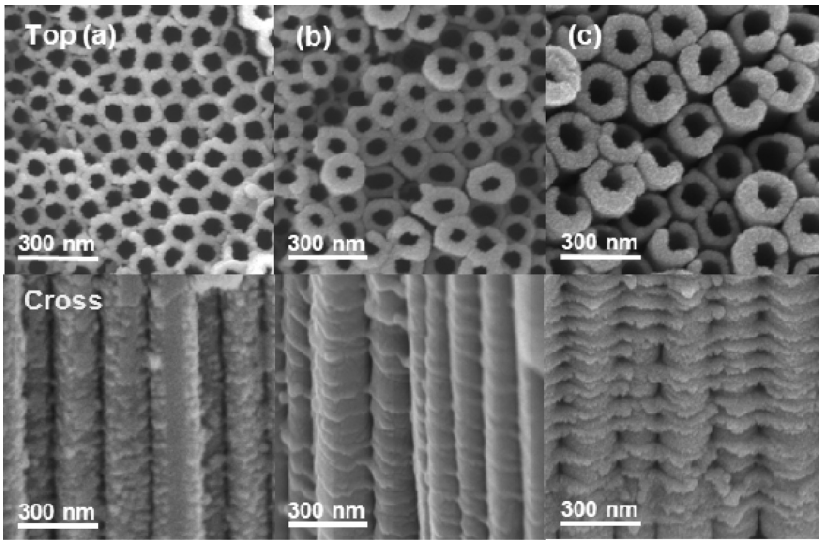

Figure 3. Top view and cross-sectional SEM images of TNT anodized at (a) 2, (b) 5, and (c) 10 wt % water in ethylene glycol electrolyte containing 0.5 wt % NaF at 60 V.

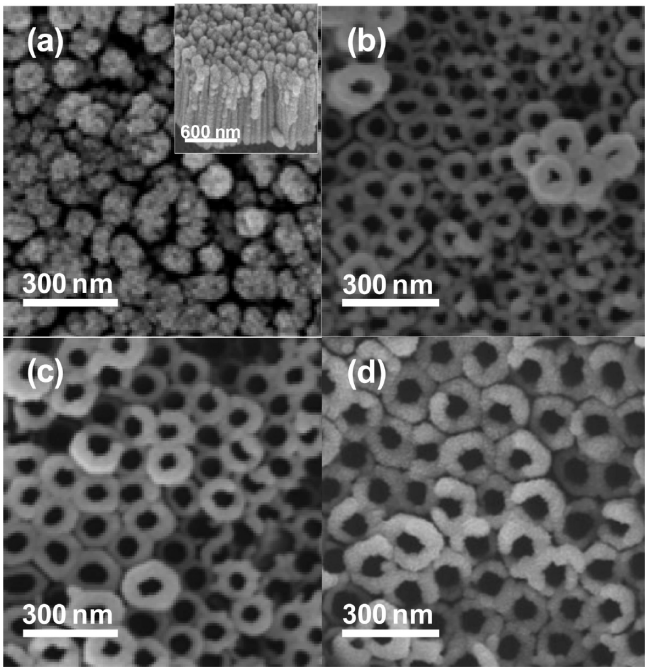

Figure 4. Top view SEM images of TNT anodized at (a) 20, (b) 40, (c) 60, and (d) 70 V in ethylene glycol containing 5 wt % water.

morphology of a membrane type TiO_2 with a long range of mesopores (Figure 3a). As nanotubes started to evolve from the electrolyte containing a larger amount of water (5 and 10 wt %), individually separated and well-oriented nanotube arrays were developed. However, TNT synthesized with 10 wt % indicates a rougher wall surface compared to others due to the extensive oxide etching. It is also interesting to note that the ripple like wall structure is observed for all samples. Although the exact mechanism is yet to be identified, the formation of ripple like surface morphology is attributed to the current oscillation during anodization. The oscillation of current occurs periodically: higher current reflects higher chemical dissolution of TiO_2 while lower current indicates the dominance of TiO_2 formation.[23,24] This current oscillation is found dependent on the water content in the ethylene glycol electrolyte. In low water concentration condition (2 wt %), the current oscillation is limited due to the slow diffusion of charges in electrolyte and vice versa for the higher water content system (10 wt %). Therefore, the TNT synthesized with higher water concentration has a more profound ripple like surface morphology, as shown in Figure 3c. To explore the optimum potential range for the TNT growth, anodization experiments with applied potential bias from 20 to 70 V were carried out in ethylene glycol containing 0.5 wt % NaF and 5 wt % water.

Figure 4 gives the corresponding SEM images of the synthesized TNT arrays. As can be seen, there is a significant effect of the potential on the morphology of TNT arrays. At a low applied potential bias of 20 V (Figure 4a), pores of nanotubes were not seen although the rod-like arrays were observed (see inset). This could be due to the fact that the entrance of the tubes was blocked by the remaining initial porous oxide layer. Because the dissolution of TiO_2 is very slow at this voltage, a longer time for the complete removal of the initial oxide layer is required.[25] As indicated in Figures 4(b−d) and Table 1, pore diameter of TNT arrays is proportional to the anodic potential, indicating a more efficient etching of the TiO_2 wall by fluoride and water at the higher applied potentials. TNT arrays prepared at 70 V gave the longest nanotube (10.6 μm) and the largest pore diameter (80.3 nm). However, the TNT array was found to peel from the Ti foil when it was subjected to a longer anodizing time. In contrast, growth of TNT at 60 V proceeds essentially proportional to the anodization time without the issue of film stability. After considering the working parameters above, an experimental condition to prepare suitable TNT arrays for DSSC application is chosen, namely fabrication in the ethylene glycol electrolyte containing 0.5 wt % NaF and 5 wt % water under the applied potential of 60 V.

Physical and Photoelectrochemical Properties of TNT arrays. Panels a and b in Figure 5 show the evolution of nanotube length, pore diameter, and wall thickness with anodization time (measured from the SEM images). The length and pore diameter

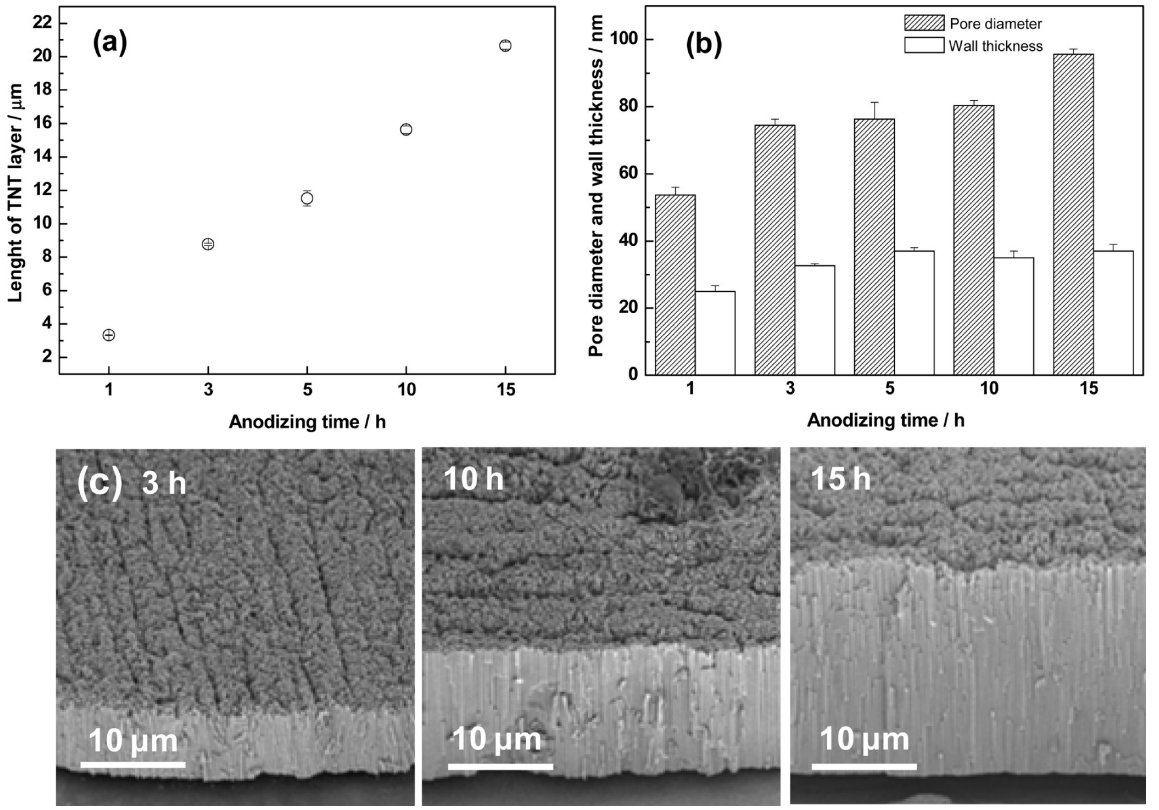

Figure 5. Geometry of TNT (a) length and , (b) pore diameter and wall thickness as a function of anodizing time. (c) Low-magnified cross-sectional SEM images of TNT anodized for 3, 10, and 15 h. Experiments were performed using ethylene glycol containing 0.5 wt % NaF.

of TNT layers substantially increases as anodization progresses. The longest nanotube with 20.6 μm was achieved after 15 h of anodization. Pore diameter also increased from 50 nm (1 h of anodization) to ~90 nm. The growth in nanotube length can be ascribed to the continuous oxidation of Ti foil, while the thinning of the tube walls is due to chemical dissolution of the oxide. As indicated in Figure 5c, homogeneous arrays of TNT over a large area of Ti foil were prepared and they exhibited consistency in nanotube length and pore diameter. However, wall thickness of the nanotube only increased until a steady-state situation established. Anodization time longer than 5 h did not further change the pore diameter and the wall thickness as shown in Figure 5b.

Figure 6a shows XRD patterns of TNT arrays on Ti foil as-synthesized and after calcinations at 450 °C for 3 h. The as-synthesized TNT arrays were amorphous contrary to the results of Schmuki et. al. who reported the formation of a trace amount of crystalline anatase phase on uncalcined TNT prepared at 40 V using NH_4F as fluoride source.[25] The amorphous phase of the as-synthesized TNT sample was transformed to mainly anatase with a trace of rutile after being calcined at 450 °C. Sodium incorporated titanate species were not observed in the XRD pattern. Since NaF was employed as the fluoride source, the possibility of the insertion of sodium or fluorine into the lattice of TNT needs to be considered. Figure 6b shows XPS spectra of the TNT array after calcination. The XPS peaks show that the anodized TNT contains only Ti (Ti 2p, 458.9 eV), O (O 1s, 530.2 eV) and C (C 1s, 285 eV) elements. As the binding energy of Ti $2p_{3/2}$ at 458.9 eV is typical to the crystalline TiO_2 structure reported in the literature, TNT is proven to be composed of Ti^{4+} bonded with oxygen after calcinations at 450 °C for 3 h.[26] The carbon element originated from the remaining ethylene glycol electrolyte, while the absence of Na proves the growth of pure TNT during anodization. Fluorine detected in the TNT array before calcination (data not shown) at 684.9 eV was attributed to physically adsorbed F^- on the surface of TiO_2. The doped fluorine from $TiO_{2-x}F_x$ species that would give rise to a peak at 688.5 eV was not observed.[27] Thus, XPS spectra confirm that doping did not occur during anodization. Optical band gap energy of the TNT arrays was calculated using the Kubelka–Munk equation to be 3.15 eV comparable to TiO_2 particles with an anatase phase (Figure 6c).

Photoelectrochemical measurements were performed using a standard three-electrode system in 0.1 M Na_2SO_4 electrolyte under UV illumination. Figure 7a shows the current-potential curves of TNT arrays synthesized from different anodization time. For all TNT arrays, the photocurrent density increased with an increase in biased potentials, whereas the dark current was negligible under scanning potentials ranging from −1.0 to 1.5 V vs Ag/AgCl. Furthermore, overall anodic photocurrent was higher for the TNT arrays synthesized from a longer anodization time due to the increase in the length of the nanotubes. The relationship between the saturated photocurrent density and the length of nanotubes is illustrated in Figure 7b. Photocurrent generation depended on the length of TNT, which is tuned by varying the anodizing time. Growth of TNT arrays represents the increase in TiO_2 surface area rendered to photoexcitation and interfaced with electrolyte. Thus it allows a higher population of electrons generated during photoexcitation to be transported to the counter electrode. Figure 7c shows the amperometry analyses of TNT arrays at 0 V vs Ag/AgCl. The short circuit current (I_{sc})

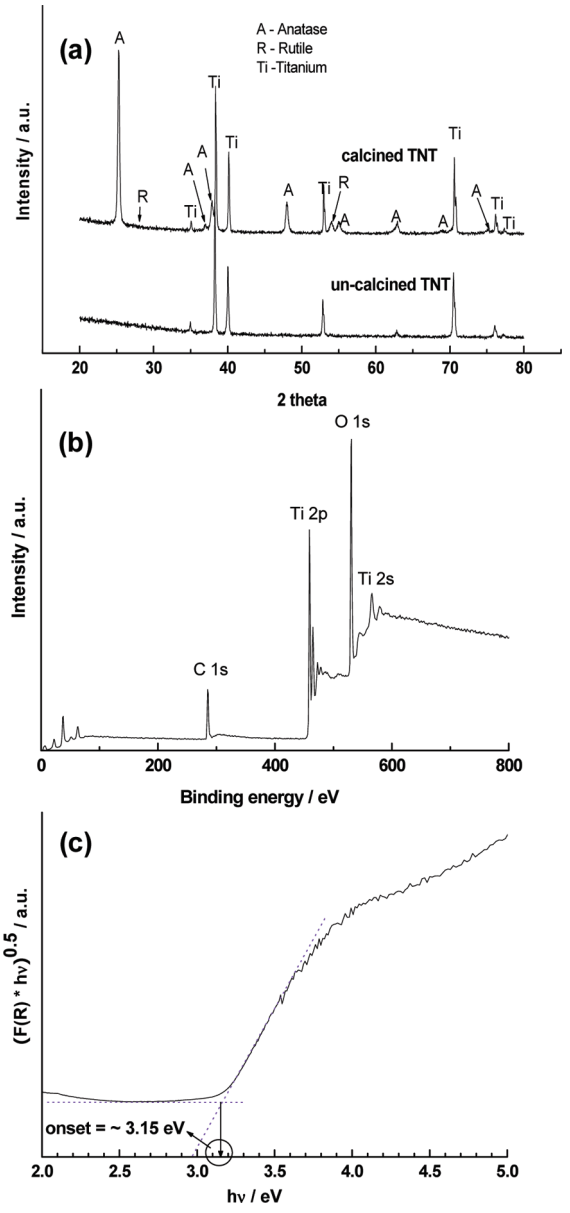

Figure 6. (a) XRD patterns of as-synthesized and calcined TNT arrays, (b) XPS spectrum, and (c) diffuse reflectance UV spectrum of calcined TNT.

generation of all TNT arrays are timely and reproducible during the repeating on-off illuminating cycles. They all exhibit a spike of photocurrent followed by decay until a steady-state is achieved. The initial spike of the current is the result of immediate separation of electron-hole pairs upon excitation, while the following recombination of the charges (hole-electron and oxidized species-electron pairs) leads to the decay of photocurrent until an equilibrium rate of the charge separation and recombination is achieved. Interestingly, when the light is turned off, the time-span for current relaxation of the TNT arrays decreased with the decrease in the nanotube length : 20.6 μm (15 h) > 15.6 μm (10 h) > 8.8 μm (3 h), as shown in Figure 7d. The decay profile of current density has been employed to describe the recombination rate in semiconductors.[28−30] This result suggests a slower recombination process occurs in the longer TNT arrays which is of importance in designing dye-sensitized solar cells as longer electron lifetime is usually a favorable property for achieving better energy conversion efficiency.

Application in Dye-Sensitized Solar Cells. The performance of the 20.6 μm (anodized for 15 h) and the 8.8 μm (anodized for 3 h) TNT array was evaluated in dye-sensitized solar cells using a N719 ruthenium-based dye as the sensitizer. Since the Ti foil is non-transparent, the sandwich type DSSCs were illuminated through the platinized ITO counter electrode (average transmission ~70% in the visible range). The current density-voltage characteristic of the solar cells (Figure 8) shows typical behaviour of an n-type DSSC with dye-sensitized TNT array acting as the photoanode. The short-circuit current density (J_{sc}), open circuit voltage (V_{oc}), fill factor (FF), and power conversion efficiency (η) are 6.71 mA cm^{-2}, 0.73 V, 0.68, and 3.33%, respectively, for the 20.6 μm TNT, and 3.00 mA cm^{-2}, 0.705 V, 0.63, and 1.37% for the 8.8 μm TNT, respectively. The efficiency of these devices are comparable to those of TNT synthesized using HF and NH_4F,[15,16,31,32] suggesting the environmentally friendly NaF as a good alternative candidate to prepare anodized TNT. Incident photon to converted electron (IPCE) measurements (Figure 9) above 500 nm shows the characteristic spectral response of N719 ruthenium dye-sensitized DSSC with maximum of 50 % at 585 nm. Below 500 nm the IPCE is rapidly decreasing due to absorption and reflection by the electrolyte layer and the platinized ITO glass. Spectral integration and overlap with a standard AM 1.5 spectrum yielded a short circuit current of 5.76 mA cm^{-2}, which is about 1 mA cm^{-2} lower than that measured using a calibrated AM 1.5 simulator. This mismatch may originate from the much lower light intensity of the IPCE setup as well as the fact that the samples for the solar cells measurements were not masked. Step-light induced measurements of photocurrent and photovoltage (SLIM-PCV)[33,34] were performed on two identically prepared samples of the best-performing DSSC using the 20.6 μm TNT array. In these transient measurements, the V_{oc} or J_{sc} decay of the DSSC is recorded in response to a stepwise change in the illumination intensity. At J_{sc}, the excess electrons between the two steady state levels of illuminations are extracted; therefore the J_{sc} decay is related to the diffusion of electrons in the TNT arrays. If charge decay due to recombination is neglected, the apparent diffusion coefficient can be calculated as

$$D = L^2(2.77\tau)^{-1}$$

where the τ is the exponent fitted to the J_{sc} decay. The calculated D values shown on Figure 10a are of a similar magnitude to mesoporous TiO_2 films[35] and increase with increasing short circuit current density. This indicates that electron transport, similarly to mesoporous TiO_2 films, is mediated by electron traps located within the gap of crystalline TiO_2. The electron lifetime is defined by the V_{oc} decay constant as measured by SLIM-PCV. The measured lifetimes on Figure 10b decrease with increasing light intensity, and are around 1 second at the lower light intensities (corresponding to about 0.6 mA cm^{-2}). The measured electron lifetimes are longer than in most mesoporous TiO_2 films indicating that the back-reaction of TiO_2 electrons with the acceptor species in the electrolyte (I_3^-) is slower. Besides, the presence of shallow surface charge trap-detrap centers as indicated in their rippled like morphology might also result in the longer electron lifetime due to the longer residence time of a trapped electron. Although this is very promising, the exact mechanism will require a

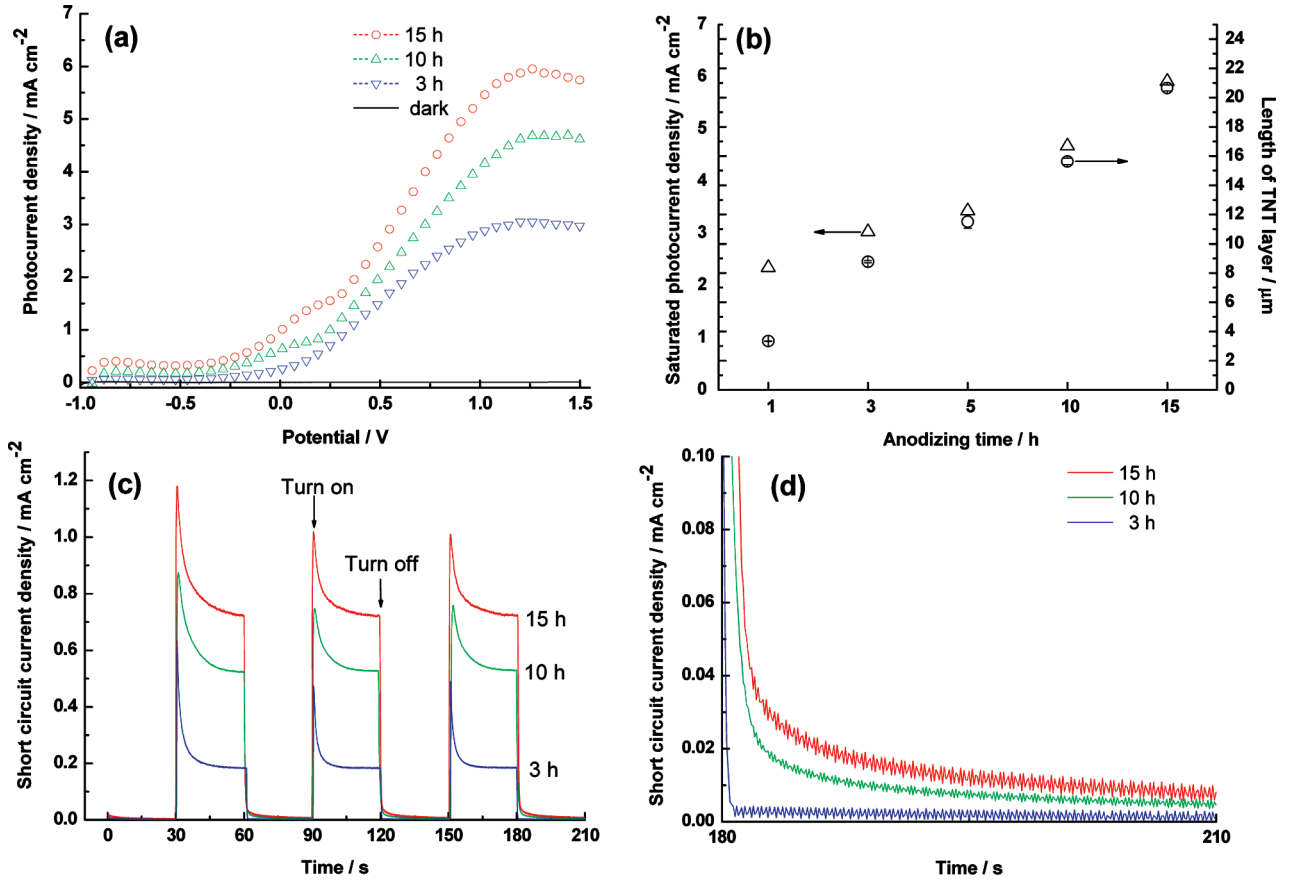

Figure 7. (a) Photocurrent−voltage relation, (b) saturated photocurrent density recorded at 1.25 V, (c) short-circuit current amperometry, and (d) current relaxation upon light-off of TNT electrodes fabricated from different anodizing time. Photoelectrochemical measurements were performed using 0.1 M Na_2SO_4 electrolyte and Ag/AgCl reference electrode under UV illumination.

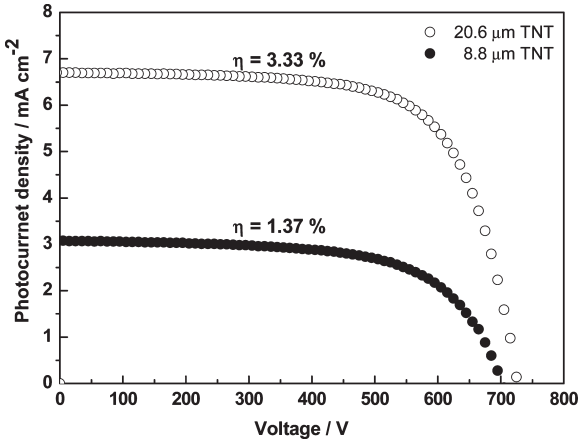

Figure 8. Current−voltage characteristics of N719 ruthenium dye-DSSCs fabricated using 20.6 μm and 8.8 μm TNT arrays treated with $TiCl_4$ under AM 1.5 solar simulator (100 mW cm^{-2}).

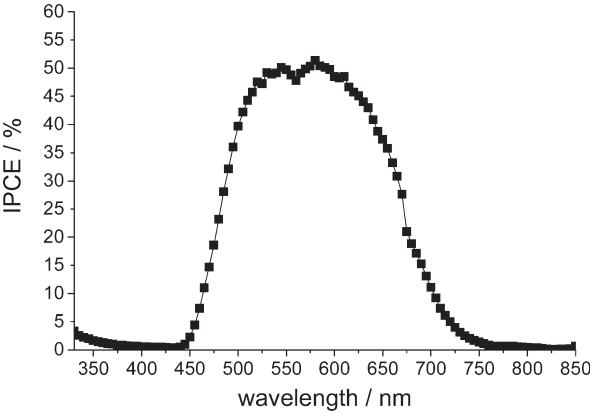

Figure 9. IPCE spectrum of the N719 ruthenium dye-DSSC using 20.6 μm TNT array.

more detailed comparison of electron lifetime and diffusion coefficient measurement at matched electron densities and as a function of TNT morphology (tube length, tube diameter, and tube wall thickness).

Finally, we have determined the open circuit voltage versus the extracted charge normalized to unit TiO_2 area using a charge extraction method. In these measurements, the photovoltage generated by illumination by a laser was carefully compensated by applying an external potential until the photocurrent was minimized (<1 μA). The light intensity and the applied voltage were switched-off simultaneously and the resulting current transient was integrated using a fast multimeter. The photovoltage is plotted versus extracted charge normalized to the unit TiO_2 volume (length of TNT array times the geometric surface area) in Figure 10c. The open circuit voltage logarithmically depends on the amount of extracted charge, which follows the frequently observed $V_{oc} \propto \log(n_{CB}/n_d)$ relationship, where n_{CB}

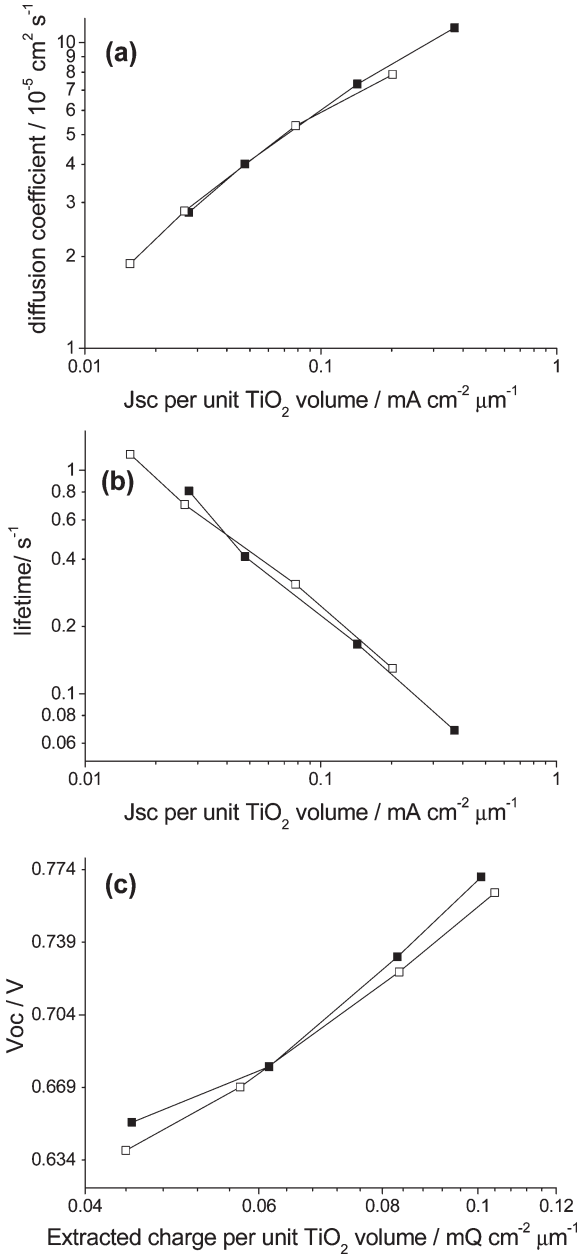

Figure 10. (a) Electron diffusion, D, coefficient; (b) electron lifetime, τ, versus J_{sc} per unit TiO_2 volume; (c) open circuit voltage, V_{oc}, versus extract charge per TiO_2 volume.

and n_d are the electron density under illumination and in the dark, respectively.[36] The light intenisity-dependent diffusion coefficient and electron lifetime suggests the presence of an exponential tail of shallow traps located below the CB level of TiO_2, and is attributed to the polycrystalline nature of the tubes.

CONCLUSIONS

Instead of hydrofluoric acid and ammonium fluoride, sodium fluoride was proven in this study to be a competent alternative and safer fluoride source to assist in the formation of titanium dioxide nanotubes using the anodization method. Unlike those short and rough nanotubes prepared in aqueous electrolyte as stringent chemical dissolution of TiO_2 occurs, the use of sodium fluoride in the organic electrolyte provided excellent control over the length and other surface morphologies of the nanotube. Geometry of nanotubes such as length, pore diameter, space between tubes and surface roughness, can be controlled by varying the electrolyte water content, anodizing voltage and duration. The effects of controlling the nanotubes morphologies, mainly the length and pore diameter, were witnessed in their photoelectrochemical behaviours and DSSCs performances. Longer nanotubes of TiO_2 not only resulted in higher photocurrent generation but also elongated the electron lifetime, which may originate from the slower back reaction and the presence of shallow surface charge trap−detrap sites. Besides having a safer source of fluoride, controlled morphology of titanium dioxide nanotubes as a tool for DSSC properties modification opens up some possibilities for designing efficient DSSCs and is worthy of further investigation.

ASSOCIATED CONTENT

Supporting Information. SEM image of TiO_2 nanotubes anodized in ethylene glycol electrolyte containing 50 wt % water and 0.5 wt % NaF. This material is available free of charge via the Internet at http://pubs.acs.org/.

AUTHOR INFORMATION

Corresponding Author
*E-mail : r.amal@unsw.edu.au (R.A.); attila@uow.edu.au (A.J.M).

ACKNOWLEDGMENT

This work was financially supported by the Australian Research Council through the ARC Centre of Excellence program. Dr. Bill Gong from UNSW Mark Wainwright Analytical Centre is gratefully acknowledged for his help in XPS measurement and analysis

REFERENCES

(1) Barbe, C. J.; Arendse, F.; Comte, P.; Jirousek, M.; Lenzmann, F.; Shklover, V.; Gratzel, M. *J. Am. Ceram. Soc.* **1997**, *80*, 3157.
(2) Gan, W. Y.; Lee, M. W.; Amal, R.; Zhao, H.; Chiang, K. *J. Appl. Electrochem.* **2008**, *38*, 703.
(3) Kang, S. H.; Choi, S.-H.; Kang, M.-S.; Kim, J.-Y.; Kim, H.-S.; Hyeon, T.; Sung, Y.-E. *Adv. Mater.* **2008**, *20*, 54.
(4) Gong, D.; Grimes, C. A.; Varghese, O. K.; Hu, W.; Singh, R. S.; Chen, Z.; Dickey, E. C. *J. Mater. Res.* **2001**, *16*, 3331.
(5) Park, J. H.; Jung, S. Y.; Kim, R.; Park, N.-G.; Kim, J.; Lee, S.-S. *J. Power Sources* **2009**, *194*, 574.
(6) Gan, W.Y.; Zhao, H.; Amal, R. *Appl. Catal. A- Gen.* **2009**, *354*, 8.
(7) Yu, J.; Yu, H.; Cheng, B.; Zhao, X.; Zhang, Q. *J. Photochem. Photobiol. A* **2006**, *182*, 121.
(8) Mor, G. K.; Varghese, O. K.; Wilke, R. H. T.; Sharma, S.; Shankar, K.; Latempa, T. J.; Choi, K. S.; Grimes, C. A. *Nano Lett.* **2008**, *8*, 1906.
(9) Paulose, M.; Shankar, K.; Varghese, O. K.; Mor, G. K.; Grimes, C. A. *J. Phys. D: Appl. Phys.* **2006**, *39*, 2498.
(10) Macak, J.M.; Tsuchiya, H.; Schmuki, P. *Angew. Chem., Int. Ed.* **2005**, *44*, 2100.
(11) Macak, J.M.; Tsuchiya, H.; Taveira, L.; Aldabergerova, S.; Schmuki, P. *Angew. Chem. Int. Ed.* **2005**, *44*, 7463.

(12) Paulose, M.; Shankar, K.; Yoriya, S.; Prakasam, H. E.; Varghese, O. K.; Mor, G. K.; Latempa, T. A.; Fitzgerald, A.; Grimes, C. A. *J. Phys. Chem. B* **2006**, *110*, 16179.
(13) Zhang, H.; Liu, P.; Liu, X.; Zhang, S.; Yao, X.; An, T.; Amal, R.; Zhao, H. *Langmuir* **2010**, *26*, 11226.
(14) Rani, S.; Roy, S. C.; Paulose, M.; Varghese, O. K.; Mor, G. K.; Kim, S.; Yoriya, S.; Latempa, T. J.; Grimes, C. A. *Phys. Chem. Chem. Phys.* **2010**, *12*, 2780.
(15) Roy, P.; Kim, D.; Paramasivam, I.; Schmuki, P. *Electrochem. Commun.* **2009**, *11*, 1001.
(16) Ghicov, A.; Albu, S. P.; Hahn, R.; Kim, D.; Stergiopoulos, T.; Kunze, J.; Schiller, C. A.; Falaras, P.; Schmuki, P. *Chem. Asian J.* **2009**, *4*, 520.
(17) Shankar, K.; Mor, G. K.; Prakasam, H. E.; Yoriya, S.; Paulose, M.; Varghese, O. K.; Grimes, C. A. *Nanotechnogy* **2007**, *18*, 065707.
(18) Paulose, M.; Shankar, K.; Varghese, O. K.; Mor, G. K.; Hardin, B.; Grimes, C. A. *Nanotechnolgy* **2006**, *17*, 1446.
(19) Yeung, C. A. *Evidence-Based Dent.* **2008**, *9*, 39.
(20) Cai, Q.; Paulose, M.; Varghese, O.K.; Grimes, C.A. *J. Mater. Res.* **2005**, *20*, 230.
(21) Kho, Y. K.; Iwase, A.; Teoh, W. Y.; Madler, L.; Kudo, A.; Amal, R. *J. Phys. Chem. C* **2010**, *114*, 2821.
(22) Giacomelli, C.; Giacomelli, F. C.; Bortolluzzi, R. L.; Spinelli, A. *Anti-Corros. Methods Mater.* **2006**, *53*, 232.
(23) Macak, J.M.; Tsuchiya, H.; Ghicov, A.; Yasuda, K.; Hahn, R.; Bauer, S.; Schmuki, P. *Curr. Opin. Solid State Mater.* **2007**, *11*, 3.
(24) Li, S.; Zhang, G.; Guo, D.; Yu, L.; Zhang, W. *J. Phys. Chem. C* **2009**, *113*, 12759.
(25) Macak, J.M.; Hildbrand, H.; Marten-Jahns, U.; Schmuki, P. *J. Electroanal. Chem.* **2008**, *621*, 254.
(26) Godfroid, T.; Gouttebaron, R.; Dauchot, J. P.; Leclere, Ph.; Lazzaroni, R.; Hecp, M. *Thin Solid Films* **2003**, *437*, 57.
(27) Yu, J. C.; Yu, J.; Ho, W.; Jiang, Z.; Zhang, L. *Chem. Mater.* **2002**, *14*, 3808.
(28) Hagfeldt, A.; Lindstrom, H.; Sodergren, S.; Lindquist, S.-E. *J. Electroanal. Chem.* **1995**, *381*, 39.
(29) Solbrand, A.; Lindstrom, H.; Rensmo, H.; Hagfeldt, A.; Sodergren, S.; Lindquist, S.-E. *J. Phys. Chem. B* **1997**, *101*, 2514.
(30) Bell, N. J.; Ng, Y. H.; Du, A.; Coster, H.; Smith, S. C.; Amal, R. *J. Phys. Chem. C* **2011**, *115*, 6004.
(31) Kim, D.; Ghicov, A.; Schmuki, P. *Electrochem. Commun.* **2008**, *10*, 1835.
(32) Kuang, D.; Brillet, J.; Chen, P.; Takata, M.; Uchida, S.; Miura, H.; Sumioka, K.; Zakeeruddin, S. M.; Gratzel, M. *ACS Nano* **2008**, *2*, 1113.
(33) Nakade, S.; Kanzaki, T.; Wada, Y.; Yanagida, S. *Langmuir* **2005**, *21*, 10803.
(34) Mozer, A. J.; Wagner, P.; Officer, D. L.; Wallace, G. G.; Campbell, W. M.; Miyashita, M.; Sunahara, K.; Mori, S. *Chem. Commun.* **2008**, 4741.
(35) Tsekouras, G.; Miyashita, M.; Kho, Y. K.; Teoh, W. Y.; Mozer, A. J.; Amal, R.; Mori, S.; Wallace, G. G. *IEEE J. Sel. Top. Quant.* **2010**, *16*, 1641.
(36) Wurfel, U.; Peters, M.; Hinsch, A. *J. Phys. Chem. C* **2008**, *112*, 1711.